

Telecom band quantum dot technologies for long-distance quantum networks

Ying Yu,¹ Shunfa Liu,¹ Chang-Min Lee,^{2,3} Peter Michler,⁴
Stephan Reitzenstein,⁵ Kartik Srinivasan,^{6,3} Edo Waks,^{2,3} and Jin Liu^{1,*}

¹*State Key Laboratory of Optoelectronic Materials and Technologies, School of Physics,
School of Electronics and Information Technology, Sun Yat-sen University, Guangzhou 510275, China*

²*Department of Electrical and Computer Engineering and Institute for Research in Electronics and Applied Physics,
University of Maryland, College Park, Maryland 20742, USA*

³*Joint Quantum Institute, NIST/University of Maryland, College Park, MD 20742, USA*

⁴*Institut für Halbleitertechnik und Funktionelle Grenzflächen (IHFG),
Center for Integrated Quantum Science and Technology (IQST) and SCoPE,
University of Stuttgart, Allmandring 3, 70569 Stuttgart, Germany*

⁵*Institute of Solid State Physics, Technische Universität Berlin, 10623 Berlin, Germany*

⁶*Microsystems and Nanotechnology Division, Physical Measurement Laboratory,
National Institute of Standards and Technology, Gaithersburg, MD 20899, USA*

(Dated: November 8, 2023)

A future quantum internet is expected to generate, distribute, store and process quantum bits (qubits) over the globe by linking different quantum nodes via quantum states of light. To facilitate the long-haul operations, quantum repeaters, the building blocks for a long-distance quantum network, have to be operated in the telecom wavelengths to take advantage of both the low-loss fiber network and the well-established technologies for optical communications. Semiconductors quantum dots (QDs) so far have exhibited exceptional performances as key elements, i.e., quantum light sources and spin-photon interfaces, for quantum repeaters, but only in the near-infrared (NIR) regime. Therefore, the development of high-performance telecom-band QD devices is highly desirable for a future solid-state quantum internet based on fiber networks. In this review, we present the physics and the technological developments towards epitaxial QD devices emitting at the telecom O- and C-bands for quantum networks by using advanced epitaxial growth for direct telecom emission, and quantum frequency conversion (QFC) for telecom-band down-conversion. We also discuss the challenges and opportunities in the future to realize telecom QD devices with improved performances and expanded functionalities by taking advantage of hybrid integrations.

I. INTRODUCTION

Emerging quantum networks^{1,2} provide unprecedented opportunities and challenges for exploring fundamental quantum physics and developing quantum technologies across a variety of the research and application frontiers such as quantum communication, quantum computation and quantum metrology. A photonic quantum network^{2,3}, as shown in Fig. 1a, consists of a global distribution of quantum information processors, quantum repeaters and quantum/classical transmission channels, in which stationary qubits are generated and processed in quantum information processors, while flying qubits (quantum states of light) transmit the quantum information through transmission channels such as the air, a vacuum of space, fiber networks or on-chip quantum circuits. The adjacent nodes and remote nodes in the quantum network are connected by quantum relays or quantum repeaters. Quantum relays are typically operated in a quantum teleportation configuration to expand the quantum communication distance between different nodes without involving quantum memories, as required for a fully fledged quantum repeater network⁴. To reach an arbitrarily long distance quantum network, quantum repeaters^{5,6}, as shown in Fig. 1b, are proposed by either employing entangled photon pairs with quantum memories or multi-photon entangled cluster graph states. In memory based quantum repeaters, a long-distance quantum channel is divided into shorter segments. Each segment is connected through entanglement swapping⁷ via Bell-state measurements (BSMs). En-

tangled quantum states are stored and purified in memories⁸ before entanglement swapping connects all these segments. To implement a quantum memory^{9,10}, a robust light-matter interface between the flying photonic states and the long-lived matter states, long storage times and multiplexed operation are required. The underlying process is often based on atomic lambda (Λ) systems (atom assemblies¹¹, nitrogen-vacancy center in diamonds¹², rare-earth ion doped solids¹³, etc.), in which the photon-spin entanglement is mapped into photon-photon entanglement. The aforementioned spin memories have been verified with high storage efficiency and long storage time¹⁰, while the orbital memories (often ladder systems) offer fast and noise-free operation¹⁴. For a recent overview and quantitative assessment of the performance of a memory-based quantum repeater system we refer to P. van Loock et al.¹⁵. In this work, the performances of basic quantum repeater links for different platforms, i.e. quantum dots (QDs), trapped atoms and ions, and color centers in diamond, are evaluated and compared for state-of-the-art experimental parameters as well as for parameters that can in principle be reached in the future. It is shown that the “repeaterless” bound in secret key rate can be exceeded for link coupling efficiencies of 60%, clock rates of 1 GHz and spin memory coherence times of 0.3 ms.

Another approach is based on all-photonic quantum repeaters¹⁶ which use logically-encoded multi-photon states such as large repeater graph states, as shown in Fig. 1c. All-photonic quantum repeaters can send and receive the heralding signals for the entanglement swapping in the same re-

peater node. The quantum nodes are linked via non-classical states of photons emitted by quantum light sources, providing redundancy against photon loss and the probabilistic nature of photonic BSMs.

To obtain long-distance quantum networks², different transmission channels depending on the required propagation distance are considered, such as optical fiber links (<500 km), fiber-based quantum repeaters (500-2000 km), satellite links (>2000 km), or some combination of these approaches. For high transmission rates, it is desirable that the quantum light sources feature very high brightness and operate at telecommunication wavelengths, i.e., within the telecom O-band (≈ 1310 nm) or C-band (≈ 1550 nm), due to the extremely-low transmission loss (0.35 dB/km at 1310 nm and 0.2 dB/km at 1550 nm) in the full-blown optical fiber links¹⁷ as well as the relatively low-background solar irradiance and Rayleigh scattering in the free-space and satellite-based quantum communication^{18,19}. Furthermore, manipulations of quantum states of light in the telecom bands can greatly benefit from the well-established technologies developed for classical optical communications and silicon photonics, e.g., high-performance semiconductor laser sources²⁰, wide-bandwidth optical modulators²¹ and high-speed photon detectors²² are readily available at telecom bands. For example, the single-photon detection efficiency as high as 93% at 1550 nm is now available through the development of superconducting nanowire single-photon detectors (SNSPDs)²³.

Semiconductor QDs exhibit exceptional performances as both quantum light sources and spin-photon interfaces for developing quantum repeaters (See Box.1). The universally used spontaneous parametric down-conversion (SPDC) and attenuated laser source in quantum communications inevitably suffer from the compromise between the source brightness and single-photon purity, which severely limits the device performance in terms of transmission distance and communication speed. In contrast, semiconductor QDs are able to generate single-photon Fock states in a deterministic manner. The state-of-the-art QD single-photon sources in the near-infrared (NIR) regime exhibit simultaneous high-degrees of end-to-end source brightness (with a record number of 57%), single-photon purity and photon indistinguishability, which already outperform SPDC sources²⁴. The benefits of exploiting QD sources as single-photon and entangled-photon pairs for quantum communications are currently under very active investigations^{25,26}. Very recent modeling suggests that a telecom band QD single-photon source featuring a collection efficiency over 30% could outperform the commercial decoy-states scheme, and the implementations of twin-field QKD protocol can further improve the QKD distance²⁶. In addition, the availability of electrical-injection of the QD source is highly beneficial for applications due to the avoidance of bulky and expensive laser system and much higher clock rates beyond 1 GHz²⁷. Towards a memory-based quantum repeater, the state-of-the-art NIR QD sources with a pair collection probability of up to 0.65(4) is one order of magnitude brighter than the SPDC source (typically with a pair

rate of <0.1)²⁸. Potentially working as a quantum memory, spin states of confined electrons/holes in QDs can be optically initialized, manipulated and read out with high-fidelity and fast-speed, which enables the realization of spin-photon entanglement²⁹ in single QDs, and even spin-spin entanglement between remote QDs³⁰. In the context of all-photonic quantum repeaters, a record-performance for the deterministic generation of photonic cluster state with an entanglement length up to 10-photons and a generation rate of 0.5 GHz was recently demonstrated in an InGaAs QD emitting at 950 nm³¹. Realistic optimizations of the sources could push the entanglement length as long as 50-photons with a generation rate as high as 2 GHz³¹. Such performances could immediately be employed to generate high-dimensional cluster states for the long-sought-after demonstrations of all-photonic quantum repeaters and distributed quantum computation. However, all the aforementioned QD devices were operated at NIR regime, experiencing an absorption at least one order of magnitude stronger than that in C-band. Thus, it is highly desirable yet challenging to transfer such exceptional performances from the NIR regime to the telecom bands for building long-distance quantum internet based on fiber networks. Here we discuss the past and on-going research activities towards semiconductor-based quantum networks and quantum repeaters in the telecom bands by exploring both advanced epitaxial growth and quantum frequency conversion (QFC). We also summarize the state-of-the-art and identify the opportunities toward real quantum networks by exploring the potential of hybrid integrated quantum photonics.

Box 1: Epitaxial QDs for quantum light sources and spin-photon interfaces

Semiconductor QDs, regarded as artificial atoms due to their discrete electronic energy levels, offer a promising way to create quantum light sources and generate light-matter entanglement in a single physical system. Single-photon generation here relies on spontaneous transitions between the discrete energy levels, with the production of a photon at each decay from an excited state (Fig. 2a). Polarization or time-bin entangled photon pairs are generated via the biexciton (XX)-exciton (X) cascade radiative processes in a single QD, as shown in Fig. 2b.

QDs feature a particularly high oscillator strength for the spin-photon interface, providing further opportunities for spin-photon entanglement generation²⁹. A single spin can be realized using a dark exciton³² or a single charge (either a hole³³ or an electron³⁴) injected into the QD by delta-doping or electrically gated-devices and can be prepared/readout via laser pulses. The spin-photon interference arises in the optical spectroscopy of a Λ system consisting of three states, which is formed in Voigt geometry under an external magnetic field (B_x) applied perpendicular to the growth direction^{33,34}, as illustrated in Fig. 2c. With the excitation of the ground state of the QD ($|\downarrow\rangle$ denotes spin antiparallel to the magnetic field) into the trion state ($|\text{Tr}\rangle$), the photon states of two different radiative recombination paths (ω_{red} and ω_{blue}) can be naturally entangled with the matter spin states ($|\downarrow\rangle$ and $|\uparrow\rangle$), creating spin-photon entangled states. The typical measurement se-

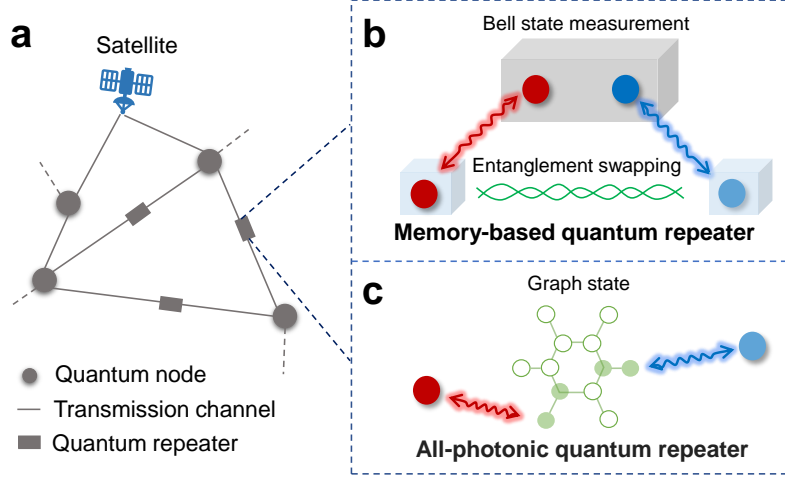


FIG. 1: **Global quantum network connected by quantum states of light.** (a) Illustration of a quantum network consisting of quantum nodes, quantum repeaters, as well as quantum/classical transmission channels; (b) Sketch of a memory-based quantum repeater, which can store and retrieve quantum information by independently creating entanglement for individual quantum nodes and then store this entanglement in quantum memory—intermediaries between different quantum systems; (c) Sketch of all-photon quantum repeater, which introduces a repeater graph state that consists of a complete connected subgraph of N core photons ($N = 6$ in our example) to implement entanglement swapping in the secondary nodes.

quence including spin initialization (I), entanglement (II), and read-out (III) is illustrated in Fig. 2d. The optical spin rotation and echo techniques (green circle) are usually explored to prolong the spin coherence time.

Linear cluster states can be generated by repeated and timed optical excitations of a confined spin in a single semiconductor QD, such as dark exciton or hole spin, as shown in Figs. 2e-f. The precessing spin will act as an “entangler” and entangles the consequently emitted photons, leading to the explicit demonstration of multi-photon-entangled cluster states^{35,36}. Both degrees of freedom, time-bin (Fig. 2e) and polarization (Fig. 2f) have been used for first demonstrations of photonic cluster states. More recently, by deterministic generation a heavy-hole spin in a QD, it was shown that entanglement can persist over ten photons, with the indistinguishability that is still keeping above 90%³¹. Spin-photon entanglement has been also injected into micropillars to generate linear-cluster states with much higher rates³⁷.

Furthermore, QD molecule devices³⁸ can also be interesting for qubit storage³⁹ and cluster-state generation⁴⁰. A single driven electron in a QD also features a collective mode of a nuclear spin ensemble that is proposed as a large nuclear spin register for quantum memory⁴¹. Moreover, the storage of deterministic single photons emitted from a QD (879.7 nm) has been demonstrated in a polarization-maintaining solid-state quantum memory based on $\text{Nd}^{3+} : \text{YVO}_4$ crystals⁴².

II. GROWTH METHODS OF QDS EMITTING AT TELECOM WAVELENGTHS

The most common approach of growing QDs is based on the Stranski-Krastanov (S-K) mode using molecular beam epitaxy (MBE) or metal-organic vapor phase epitaxy (MOVPE). Two material systems are exploited to shift the emission wavelength from the NIR to the telecom O- and C-bands: $\text{In}(\text{Ga})\text{As}/\text{GaAs}$ and InAs/InP . However, in general the self-assembled S-K growth method results in randomly positioned QDs with a significant inhomogeneous broadening of the QD emission range. This inhomogeneity, together with the random positions, strongly impair the production yield of devices based on single QDs, imposing a formidable challenge to the scalability. Thus, in addition to S-K growth mode, we will also address droplet epitaxy, which significantly reduces the QD density, the lattice strain and the exciton fine structure splitting (FSS) for polarization-entangled photon pair generation, as well as site-controlled growth, which overcomes the spatial randomness of S-K growth mode.

A. Stranski-Krastanov growth

$\text{In}(\text{Ga})\text{As}/\text{GaAs}$ QDs. The lattice mismatch between InAs and GaAs is 7.2%, inducing a typical emission wavelength of ≈ 920 nm at 4K. To redshift the ground-state transition energy of $\text{In}(\text{Ga})\text{As}$ QD from the NIR to the telecom spectral range, the primary approach is to decrease the lattice mismatch for increasing the QD size. One concept is to apply a strain-reduce layer (SRL) on the top of $\text{In}(\text{Ga})\text{As}$ QDs during growth to minimize strain and surface energy⁴³. An $\text{In}_x\text{Ga}_{1-x}\text{As}$ ($0.1 < x < 0.3$) layer, shown in upper left of

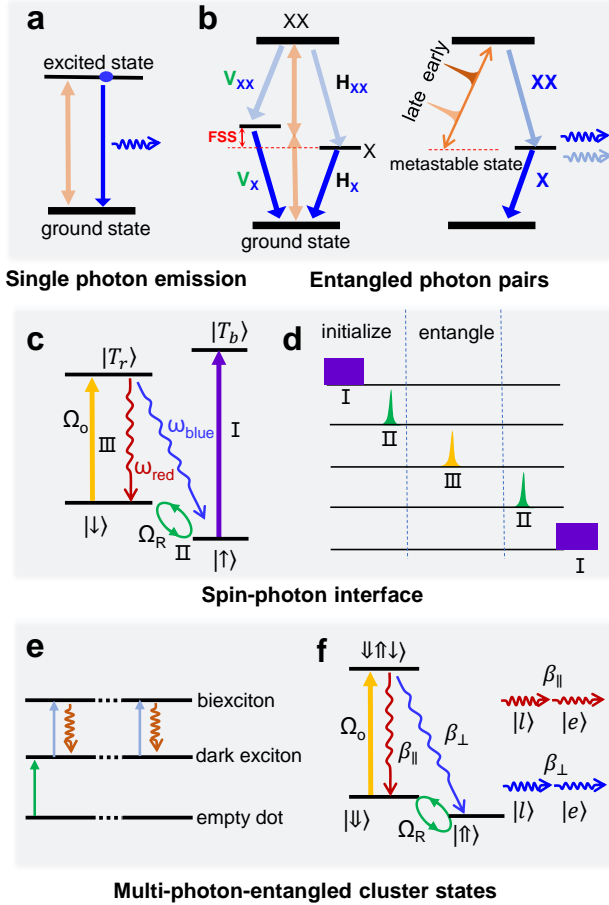


FIG. 2: **Epitaxial quantum dots (QDs) for building quantum nodes.** (a) Illustration of a single photon generated via spontaneous radiation between the discrete energy levels in a single QD; (b) Illustration of polarization (left) or time-bin (right) entangled photon pairs generated via the biexciton (XX)-exciton (X) cascaded radiative processes in a single QD; (c) Photon-spin interface in a single QD with a two- Λ energy-level diagram and the allowed optical transitions in Voigt geometry under an external magnetic field (B_x) applied perpendicular to the growth direction; (d) Timing diagram of the pulse sequence for the spin-photon interface in QDs, including spin initialization (I), entanglement generation (II), and spin read-out (III); (e-f) Multi-photon-entangled cluster states created in a single QD by using a dark exciton³⁶ (e) or a hole spin³⁵ (f). In (e) the cluster state is based on polarization entanglement and in (f) on time-bin entanglement. The wavy arrows in (a-f) represent photons. Images in (e-f) are adapted with permission from Refs. [35,36], respectively.

Fig. 3a, is used to cover the QDs instead of capping with GaAs after the formation of QDs⁴⁴. Single-photon emission with a high multi-photon suppression of $g^{(2)}(0)=0.027 \pm 0.005$, and a post-selected visibility of 96% (raw visibility: 12%) was reported, using InAs QD with SRL (telecom O-band) combined with p shell excitation⁴⁵. Another option to redshift to telecom wavelength is capping InAs QDs with a thin GaAs_{1-x}Sb_x layer⁴⁶. However, the QD linewidths are ≈ 3 -5 meV, which attributed to more fluctuating carrier occupancy of states in InAs/GaAs_{1-x}Sb_x system with type-II band energy, leading

to low-coherence photons.

Another approach is to increase the lattice constant of the buffer layer below the QDs, as presented in upper right of Fig. 3a. In this case, the InAs QDs are deposited on an InGaAs metamorphic buffer layer (MMBL)⁴⁷. The lattice mismatch between In_xGa_{1-x}As and InAs is reduced by increasing the indium content of MMBL, resulting in larger dot size and lower band gap of the QD material which allows to reach emission in the telecom C-band⁴⁸. Alternatively, strain-coupled bilayer QDs (BQDs), shown in bottom left of Fig. 3a, can be introduced⁴⁹. As its name suggests, two vertically coupled QD layers separated by a thin GaAs or Al_xGa_{1-x}As spacer layer (with a thickness of less than 10 nm) are implemented to increase the actual size of the QDs and therefore extend the wavelength to the telecom O- and C-bands. Combined with a resonant pumping scheme, an on-demand single-photon source⁵⁰ and entangled photon pair source⁵¹ based InAs/GaAs QDs with MMBLs emitting in the telecom C-band, have been demonstrated.

InAs/InP QDs. Compared with lattice mismatch (7.2%) in InAs/GaAs QDs, the lattice mismatch between InAs and InP is much smaller (3.2%). Thus, this type of InAs QDs is an interesting candidate to emit single photons at the telecom C-band without any strain engineering layer. However, the smaller lattice mismatch also results in high QD density (often larger than 10^{10} cm^{-2})⁵² and relatively large QDs (with emission beyond 1600 nm at room temperature⁵³), as well as As/P exchange at the InAs/InP interface⁵⁴. A growth method based on ripening of InAs quantum sticks (QSs), which is triggered by the sample cooling under arsenic overpressure, has been developed to reduce the QD density⁵⁵. Additionally, an ultrathin interlayer (In_xGa_{1-x}As or InAlGaAs) underneath the InAs layer⁵⁶ or double-InP-capping method⁵⁷ can be introduced to achieve the C-band emission, as illustrated in bottom right of Fig. 3a. The latter approach can also reduce QD density and suppress the As/P exchange at the InAs/InGaAsP interface.

B. Droplet epitaxy

Due to the high density of InAs/InP QDs in S-K growth mode of typically larger than 10^9 cm^{-2} , sub- μm photonic structures are often employed to realize single-QD devices⁵⁷. In this context, droplet epitaxy (DE) is a very promising alternative to the conventional S-K mode growth⁵⁸. It starts by depositing group III atoms at controlled temperature and flux to form droplets with appropriate density and size on the substrate, followed by a group V deposition to crystallize the initial droplets into III-V islands directly (Fig. 3b). DE QDs have higher structural symmetry and, thus, lower FSS if compared with S-K QDs, which facilitate the generation of polarization-entangled photon pairs⁶⁰. Single photons⁶¹ and entangled photon pairs⁶² in the C-band have been reported using InAs DE grown on InP by MOVPE and MBE. It is further noted here that also InAs DE QDs grown on InP (111)A, a substrate which has C_{3v} crystal symmetry, have the advantage of high

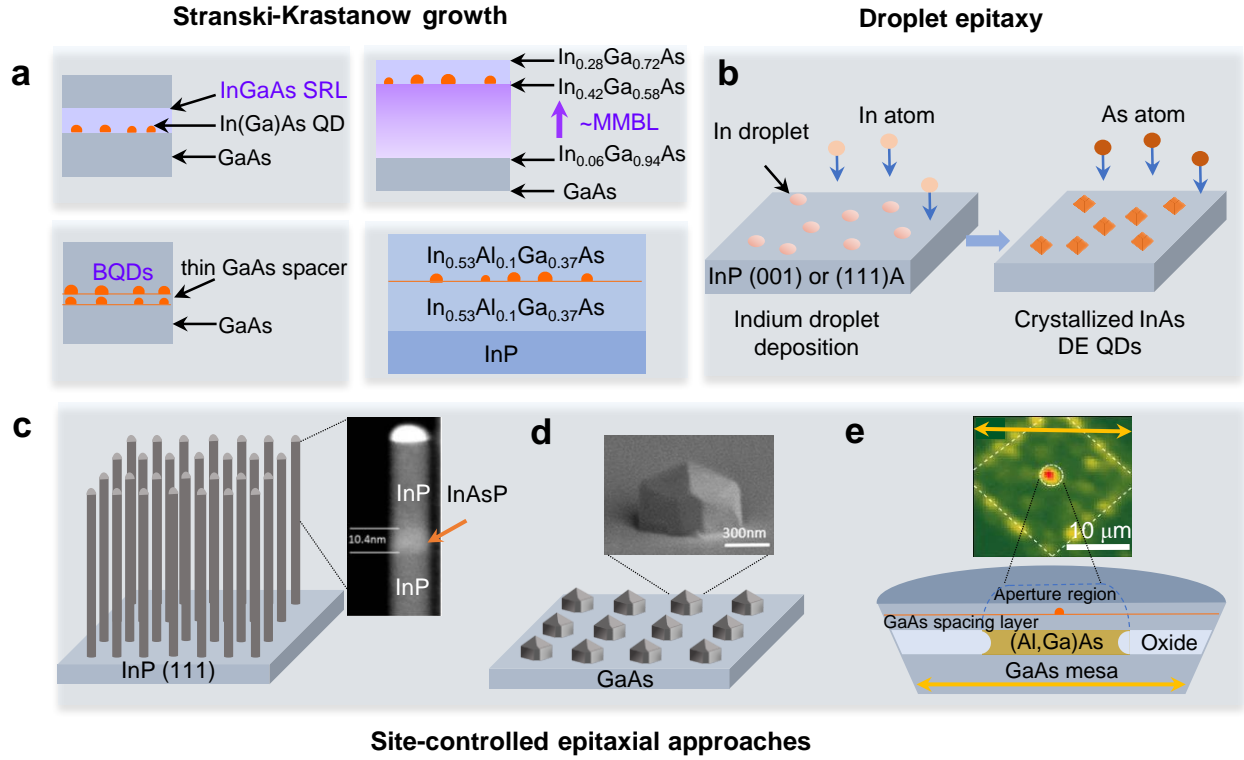


FIG. 3: **Epitaxial growth for telecom QDs.** (a) Sketches of Stranski-Krastanow growth of QDs emitted at telecom wavelengths, including (1) InGaAs QDs with InGaAs SRL (upper left), (2) InAs QDs above a metamorphic InGaAs matrix (upper right), (3) bilayer QDs (bottom left) and (4) InAs/InAlGaAs/InP QDs (bottom right); (b) Schematic of growth and fabrication stages of droplet etching (DE)-based QDs. (c) Schematic of InP nanowires arrays grown on InP (111)B. Each photonic nanowire waveguide contains a single InAsP/InP QD, together with a high angle annular dark field (HAADF) scanning TEM image of an $\text{InAs}_{0.5}\text{P}_{0.5}$ QD in InP nanowire⁶⁹. (d) Schematic of a mesa-top single QD (MTSQD) array. A magnified SEM of a single mesa bearing MTSQD is shown in the upper SEM image⁷⁰; (e) Schematic of the buried-stressor structure⁷¹, together with the micro-PL mapping results after the site-controlled growth⁷²; Reprinted with permission from Refs. [69–72]

symmetry and low FSS⁶³. Entangled photon pair emission by InAs/InP DE QD with a fidelity of $(87 \pm 4)\%$ was reported with emission at 1550 nm ⁶², highlighting a viable path to the QDs-based entangled light sources at telecom wavelength for long-distance quantum network applications.

More interestingly, the so-called “nanodrill” effect of group III droplets at high growth temperatures can be used to create arrays of local droplet etching (LDE) nanoholes that serve as growth templates for QDs. In contrast to the S-K concept, this method does not rely on lattice mismatch between the matrix and QD materials and thus allows for the growth of the strain-free QDs, such as highly symmetric GaAs/AlGaAs QDs. The reported GaAs QDs (emitting at $\approx 780 \text{ nm}$) that formed in the defect and impurity-free Al-GaAs nanoholes, yield almost diminishing FSS leading to excellent entangled photon pair generation with an entanglement fidelity of $0.88(2)$, and a high single photon indistinguishability of $0.903(3)$ ²⁸. By embedding GaAs QDs into an n-i-p-diode, single-photon emission with close-to lifetime-limited linewidths and no-blinking, as well as an electron spin initialization with high fidelity and a spin-relaxation time as large as $50 \mu\text{s}$ are achieved⁶⁴. For high performance LDE QD emitting at the telecom wavelength, GaSb/AlGaSb⁶⁵ or

In(Ga)As/InAlAs/InP⁶⁶ materials will have the opportunity to be established and engineered to the growth of lattice-matched and defect-free QDs.

C. Site-controlled growth

Due to the self-assembled mechanism, S-K and DE growth modes result in randomly positioned and highly inhomogeneous QD populations. This makes the fabrication of single QD devices with a high scalability very challenging and has led to the development of advanced deterministic QD-device fabrication technologies⁶⁷. Overcoming spatial and spectral inhomogeneities already at the growth stages would constitute a major breakthrough, and new site-controlled growth methods may provide a pathway to realize the atomic-scale control for ultimate spectral engineering of QDs. A QD in a nanowire (NW) structure⁶⁸, promises a high position accuracy because these emitters can grow using a combination of selective-area and vapour-liquid-solid (VLS) epitaxy on patterned [111]-oriented substrates (Fig. 3c). The most popular configuration consists of a QD embedded on the NW axis as a disk, forming an axial heterostructure of the type A/B/A, where B shows

quantum confinement. Core-shell structures are also implemented to protect the QD from the surface states, which can degrade the optical properties of the NW-QD through nonradiative recombination and spectral diffusion. Notably, single InAsP QDs-in-NWs have exhibited the ability of producing bright single-photon emission with an unprecedented spectral range from 880 nm to 1550 nm⁶⁹.

Other site-controlled epitaxial approaches, which have been successfully applied to (In)GaAs/GaAs QDs emitting at $\lambda < 1000$ nm, may provide further opportunities for pursuing QDs emitting at telecom wavelengths. The first promising technique is spatially selective growth using substrate-encoded size-reducing epitaxy (SESRE) on spatially regular arrays of patterned nanomesas, as shown in Fig. 3d, which enabling single QD arrays with spectral uniformity of ≈ 5 nm⁷⁰. Another improved site-controlled technology is based on the buried-stressor growth⁷¹. Here, local strain-engineering by an oxide-aperture leads to the localized formation of single QDs, as illustrated in Fig. 3e. Tight site-control, very good optical properties and even resonance fluorescence have been observed for buried-stressor InAs/GaAs QDs emitting at 920-950 nm⁷², and it will be interesting to further develop this technique for realizing site-controlled QDs in the O-band by combining it for instance with the SRL concept.

III. COUPLING TO TELECOM BAND SINGLE-MODE FIBERS

The underlying philosophy in developing telecom band QDs is to take advantage of the mature optical fiber networks to expand the transmission distance of quantum information. For example, the 3 dB propagation distance in single mode optical fiber at 1550 nm is 15 km, while in the 900 nm band it is ten times smaller. Therefore, the single-photons and entangled photon pairs emitted by the telecom-band QDs have to be engineered to force its non-directional spontaneous emission into one specific mode that can then be coupled into a fiber. This can be achieved using microcavities, which enhance the coupling between the QD dipole and the electromagnetic mode confined in the cavity, or with waveguides, which inhibit the emission outside of the waveguide mode. For efficient coupling to fiber, one can first extract the photons to free-space and subsequently couple the far-field emission into single-mode fibers (most natural for geometries that typically emit into free-space, such as micropillars or circular Bragg gratings (CBGs) or instead directly couple the photons to single-mode fibers via near-field coupling (most natural for QDs that emit into in-plane geometries such as photonic crystals or suspended channel waveguides). Both strategies heavily rely on the engineering of the radiation characteristics of QDs by using photonic nanostructures.

A. Extraction to free-space for fiber coupling

The photonic nanostructures for extracting light to the free-space or into optical fibers fall into three categories: optical

microcavities, photonic waveguides and lens-based geometry, as schematically shown in Fig. 4a-c respectively. An optical microcavity features an advantage of both improving the photon extraction efficiency and accelerating the spontaneous emission rate via the Purcell effect. Microcavities based on pillars⁷³, photonic crystal defects⁷⁴⁻⁷⁶ and CBGs⁷⁷⁻⁸¹ have been successfully employed to develop bright single-photon sources at both O- and C-bands. In particular, L3 type photonic crystal cavity in O-band exhibits a photon extraction efficiency of $(36 \pm 5)\%$, a high purity of 91.5% and a high post-selected indistinguishability of 67% (raw visibility: 18%)⁷⁵, while the O-band (C-band) CBG shows a photon extraction efficiency of 23%⁷⁸ (16.6%⁸¹), a low $g^{(2)}(0)$ of 0.01⁷⁸ (0.003⁸¹) with a raw indistinguishability of 19.3%⁸¹. Recently, a simultaneous high-brightness with a fiber-coupled single-photon rate of 13.9 MHz for an excitation rate of 228 MHz has been demonstrated with a CBG while maintaining a low multi-photon contribution of $g^{(2)}(0) = 0.005$ ⁸⁰. In a wide-band photonic waveguide⁸²⁻⁸⁶, spontaneous emission to the radiation modes are greatly suppressed and can only couple to the propagating waveguide mode, improving the photon extraction efficiency with a record value of 27% for waveguide sources at O-band⁸⁶. Without modifying the spontaneous emission dynamics, solid immersion lenses (SILs)⁸⁷, as well as microlens/micromesa-based structures^{88,89}, are another alternative to increase the photon extraction efficiency over a broadband range. Such structures can shape the propagation of the emitted photons, effectively guiding the photons towards the top collection optics. High experimental photon extraction efficiency of 17% has been reported when GaP SILs⁸⁷ or microlens⁸⁸ are applied to enhance photon extraction of O-band InGaAs/GaAs QDs.

The above has focused on the photonic geometries used to extract QD emission into free-space before coupling into a fiber, and many efforts continue to determine how to best optimize such structure⁹⁰. Of additional importance are the methods for on-chip fiber coupling, in some cases using free-space micro-optics (i.e., lenses) for mode matching, so that user-friendly fully fiber-coupled sources suitable for alignment-free operation can be realized. One process to realize such functionality is based on active optical alignment and epoxide adhesive bonding at room-temperature⁹¹, as shown in Fig. 4d. Using this process, A. Musial et al. deterministically integrated a QD into a micromesa and on-chip coupled to a high numerical aperture (NA) customized single-mode fiber. The realized source can deliver a single-photon emission rate of up to 73 kHz in an application oriented stand-alone device⁹².

B. Direct evanescent fiber coupling

Alternately, single photons emitted by QDs could be directly coupled to optical fibers relies on evanescent wave interactions. When the modes of the two waveguiding structures (one the QD-containing semiconductor waveguide, the other the optical fiber) can be phase-matched, appreciable power

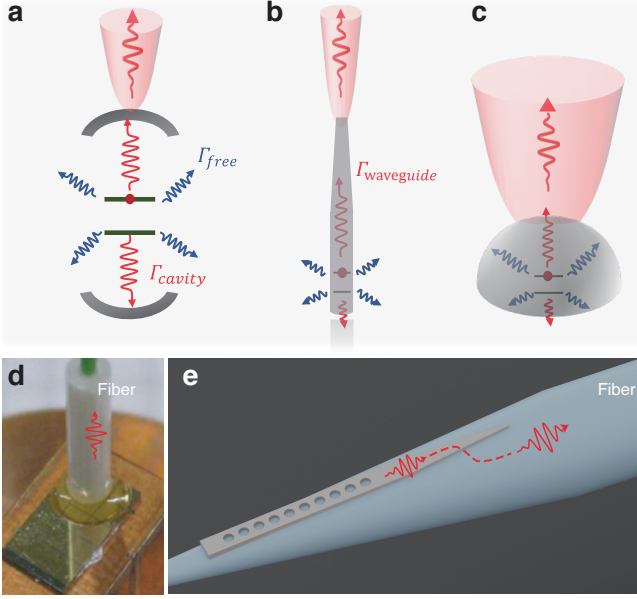


FIG. 4: **Coupling telecom band quantum light sources into single-mode fibers.** (a) Sketches of microcavities used for extracting single photons from semiconductors and coupling into single-mode fiber. The red arrows point out the photon extraction directions, while the blue arrows represent spontaneous emission in other directions; (b) Sketches of photonic waveguides, in which the photons predominantly funnel to the fundamental waveguide mode with high-efficiency light extraction (red arrows). The waveguide end can be carefully tapered to lead the mode to adiabatically expand outside and form a Gaussian-like far-field pattern that can be efficiently collected by a single-mode optical fiber; (c) a typical micro-lens geometry, which can shape the propagation of the emitted photons, effectively guiding the photons towards the top collection optics (red and blue arrows); (d) Photograph of a fiber-coupled QD sample after the epoxide adhesive bonding process⁹¹; (e) Schematic of the integrated photonic crystal nanobeam and the fiber taper for near-field couplings. Reprinted with permission from Ref. [91].

transfer - in principle 100% - can be achieved with sufficient transverse mode overlap and interaction length along the propagation direction⁹³. To realize appreciable transverse mode overlap, tapered optical fibers can be utilized to extract single photons confined in semiconductors into telecom band single-mode fibers. C. M. Lee et al.⁹⁴ demonstrate an alignment-free fiber-coupled SPS at telecom wavelength with a brightness of 1.4% via transferring a PC nanobeam to a tapered optical fiber, as illustrated in Fig. 4e. This evanescent coupling scheme can also be implemented in NW waveguides⁹⁵, with a source fiber collection efficiency of 35% and an overall single photon collection efficiency of 10%. It is important to note that the direct, on-chip fiber coupling approach usually suffers from much lower additional loss than a typical free space photoluminescence setup, thereby resulting in a similar detected photon flux. Finally, such approaches can be readily applied to QD-containing cavities; the fiber taper can be directly coupled to the cavity, as in Ref.⁹⁶, or instead coupled to an on-chip waveguide that is in turn coupled to the cavity, as has been demonstrated in the context of other integrated photon-

ics experiments, where fiber-to-cavity coupling efficiencies as high as 85% have been shown⁹⁷.

IV. STATE OF THE ART OF EPITAXIAL TELECOM WAVELENGTH QUANTUM LIGHT SOURCES AND SPIN-PHOTON INTERFACES

In the previous sections, we have extensively discussed techniques used to engineer the extraction efficiency and the in-fiber brightness properties of QDs emitting at telecom wavelength. However, the brightness, single-photon purity, and indistinguishability of telecom band QD SPSs, have only been demonstrated separately in previous experiments. Recent experiments exploiting advanced excitation schemes, as summarized in Table I., have demonstrated steady improvements of the device performances, as compared with the QD-based quantum light sources that emitted in the NIR regime.

Epitaxial telecom wavelength quantum light sources have been applied in some proof-of-principle experiments of implementing quantum networks, for example, distributing single photons⁹⁸ and entangled photons^{99,100} over deployed telecom fiber that enable wavelength division multiplexing, teleporting with telecom-wavelength polarization-encoded laser qubits¹⁰¹, random number generation⁹⁸, and GHz-clocked quantum relays²⁷. These QD-in-phonic structures were further used to demonstrate hundreds of kilometers QKD¹⁰², overcoming the distance limit of a weak coherent pulse (WCP) source (without decoy states) and a QD-generated single-photon pulse at a wavelength of 900 nm.

There are still a few remaining issues to be solved before obtaining the all-round SPSs at telecom band for multi-photon applications and long-haul entanglement distribution in quantum networks. First, the demonstrated collection efficiency into the first lens is limited by 36%⁷⁵, hybrid CBG devices in which a CBG sits on top a thin SiO₂ spacer layer with a gold reflector are being exploited for reaching a collection efficiency into the first lens towards 80%¹⁰³. Second, most of the reported QD sources at telecom bands featured appreciable blinking and spectral diffusion, which is probably due to the fluctuating charge environment. A p-i-n diode design with ability of tuning the charge states of the QDs and stabilizing the surrounding charged environment is supposed to solve the problem, and there have been significant efforts towards this direction in the community^{24,104}. Finally, two photon interference (TPI) with a long-time delay is essential for scalable photonic quantum applications. Telecom single photons with coherence times much longer than the Fourier limit and TPI after 25 km fibre spool¹⁰⁵ have been demonstrated on InAs/InP QD platform. Taking a further step, charge environment control using the p-i-n diode⁶⁴ and fast photon emission from Purcell enhancement¹⁰⁶ is expected to enable the long-time delay TPI. For entangled photon pairs at telecom wavelengths, a step forward is fine-structure suppression for S-K type QDs using micro-machined piezoelectric actuators¹⁰⁷, which improving the fidelity of entangled state.

One exciting progress in the community is the very recently demonstrated C-band spin-photon interface based on single

TABLE I: State of the art of single-photon sources and entangled photon pair sources based on epitaxial quantum dot

	Wavelength	QDs and growth methods	Photonic structure	Excitation schemes	Photon extraction efficiency	$g^{(2)}(0)$	Indistinguishability with/without a post-selection	Ref.
Single-photon sources	O-band	InAs/InP, S-K	Photonic crystals	wetting layer	$(36 \pm 5)\%$	0.085 ± 0.022	$(67.0 \pm 2.0)\% / (18.0 \pm 1.0)\%$	⁷⁵
	O-band	InAs/InP, S-K	Nanobeam	p-shell	$(27.0 \pm 0.1)\%$	0.077 ± 0.011	$(91.0 \pm 9.0)\% / (20.0 \pm 4.0)\%$	⁸⁶
	O-band	InGaAs/GaAs, SRL	Microlens	wetting-layer	$(17.8 \pm 3.8)\%$	0.21 ± 0.07	-	⁸⁸
	O-band	InGaAs/GaAs, SRL	SIL	above-band	17%	0.049 ± 0.02	-	⁸⁷
	O-band	InGaAs/GaAs, SRL	CBG	p-shell	23%	0.01	-	⁷⁸
	C-band	InAs/InP, S-K	CBG	LO-phonon-assisted	$(16.6 \pm 2.7)\%$	0.0032 ± 0.0006	$(99.8^{+0.2}_{-2.6})\% / (19.3 \pm 2.6)\%$	⁸¹
	C-band	InGaAs/GaAs, MMBL	CBG	p-shell	17%	0.005	-	⁸⁰
	900 nm	InAs/GaAs, S-K	Open Fabry-Perot cavity	resonance excitation	$(82 \pm 2)\%$	0.0021	- / 96.7%	²⁴
	Wavelength	QDs and growth methods	Excitation schemes	Photon pair generation efficiency	Peak fidelity	A pair collection probability	Indistinguishability	Ref.
Entangled photon pairs	C-band	InAs/GaAs, MMBL	TPE	$(69.9 \pm 3.6)\%$	$(95.2 \pm 1.1)\%$	-	-	⁵¹
	780 nm	GaAs/AlGaAs, DE	TPE	90%	$(88 \pm 2)\%$	$(65 \pm 4)\%$	$(90.3 \pm 0.3)\%$	²⁸

InAs/GaAs QD grown on an MMBL¹⁰⁸. The optical spin injection, initialization, read-out, and full coherent control of a confined hole are realized by using picosecond optical pulses. The dephasing time was limited to 240 ps which could be significantly improved in the future for spin-photon and spin-spin entanglement. Integration of QDs into photonic nanostructures can also further significantly enhance the spin-photon coupling and improve the performance of quantum interfaces.

V. QUANTUM FREQUENCY CONVERSION OF SINGLE QDS TO TELECOM WAVELENGTHS

Despite the significant progress that has been made in shifting the emission wavelength of the QD emitters to the telecom band via controlling the epitaxial growth processes, the above-mentioned QDs emitting at telecom bands are generally less mature than their shorter wavelength counterparts, and thus often suffer from high dislocation densities or impurity concentration, resulting in high charge noise, blinking, and therefore low photon indistinguishability. Another route to bridge the frequency gap is QFC, which can convert NIR single photons to the telecom wavelengths while preserving its superior quantum optical properties, been implemented in different quantum systems to realize spin-photon¹⁰⁹/photon-photon entanglement¹¹⁰ or access to quantum memory¹¹¹ at

telecom range. Compared with other wavelength-tuning approaches used in QD systems such as temperature, electric field or strain, QFC does not influence the emission process itself and therefore can be applied to transfer single photons over a wider spectral range. For quantum internet applications, firstly, QFC can translate the mature NIR single photon to telecom wavelengths with high efficiencies and low noise, allowing high quality SPSs for long-distance QKD. Secondly, QFC can erase the frequency difference and spectral distinguishability among different QDs or with other quantum nodes, which is essential for TPI, a core ingredient in entanglement swapping protocols that, for example, extend the distance of a quantum link. Most importantly, both QD-based quantum devices and QFC modules are increasingly being realized with mature, semiconductor-based planar fabrication technology, making them particularly appealing for on-chip integration.

In this section, we will focus on the near-visible-to-telecom QFC technologies that are suitable for QD quantum light sources, including the second-order nonlinear process based on mature, cm-scale periodically poled lithium niobate (PPLN) waveguides as well as the third-order nonlinear process based on emerging, ultra-compact chip-integrated microresonators (SiN_x, AlN, AlGaAs, etc.) which have great potential for implementing QFC on a chip and the possibility of scalability and integration with other chip-integrated pho-

tonics.

A. QFC based on cm-scale PPLN waveguides

The QFC enables changing the frequency of the photonic qubits (i.e., the QD SPS, also referred to as the ‘signal’) to the target output frequency (‘idler’) while preserving the quantum information they encode¹¹². PPLN waveguides have served as the most popular choice for QFC. As illustrated in Fig. 5a, the QFC is done through the second-order nonlinear process with a $\chi^{(2)}$ nonlinearity in a three-wave mixing process, where a single-photon input is mixed with a strong pump laser beam to produce a single-photon output at either the sum or difference frequency. Such a technique has been widely applied to down-shift single photons emitted by QDs to the telecom C-band, where the use of a long wavelength pump near 2000 nm ensures limited noise photon generation. The best reported end-to-end system efficiency is 40.8% and with a high purity of 97.6% and a high degree of indistinguishability of 94.8%¹¹³. QFC enabled by the PPLN waveguide has also been used to convert two single photons with an appreciable energy difference from 910 nm to 1560 nm single photons, which erases the which-way frequency information and enabled the realization of spin-photon entanglement¹¹⁴.

Via the QFC technique, TPIs in the telecom C-band by exploiting QFC on two remote QD emitters were reported with increasingly improved performances^{110,115}. A very desirable forward step in QFC is the development of techniques capable of converting one photon of an entangled photon pair source to the telecom bands for entanglement swapping between remote QDs, as illustrated in Fig. 5b. The most crucial issue is to preserve the input polarization states. A polarization-insensitive QFC (PIQFC) can be implemented, in which a PPLN waveguide is installed in a Sagnac interferometer¹¹⁶. Moreover, applying QFC on the photon part of the spin-photon entanglement for TPI interface over the long fiber links could enable the generation of entanglement between remote local solid-state spin qubits, showing prospects for the implementation of quantum memories and multi-photon-entangled cluster states.

B. QFC based on integrated nanophotonics

Notably, the strong pump power (on the order of a few hundred mW) and a relatively large size (waveguide length on the order of cm) required by the conventional PPLN can be alleviated by the integrated photonic approach^{117,118}. In contrast, the large refractive index difference between the nanophotonic waveguide material and the underlying insulator provides tight optical confinement, strong mode overlaps, and new opportunities for dispersion control¹¹⁹. The microring cavity-based structure can further boost the efficiency of

second-order or third-nonlinear processes and therefore reduce the required pump power to levels consistent with low power, continuous-wave lasers.

Among the material platforms widely employed in integrated photonics, silicon nitride SiN_x ¹²⁰ offers broadband optical transparency, relatively high optical nonlinearity, and low linear and nonlinear absorption, which is particularly suitable for QFC experiments. Four-wave mixing Bragg scattering (FWM-BS), a third-order nonlinearity ($\chi^{(3)}$) process, has been under heavy investigations for low-noise QFC firstly in the optical fibers¹²¹ and then in chip-scale devices¹¹⁸. In comparison to four-wave mixing processes based on parametric amplification that are often used in classical applications where the generation of added noise photons may not be as important, FWM-BS directly converts signal photons to idler photons, and has no fundamental additive noise floor, thus making it particularly suitable for QFC. As illustrated in Fig. 5c, the signal photon will be ‘scattered’ to idlers (in the frequency domain), with the frequency shift determined by the frequency difference of the two nondegenerate pump lasers. By carefully engineering the phase matching conditions and employing cavity-enhancements, efficient and low-noise intra-band (few nanometers spectral shift) and inter-band (few hundred nanometers spectral shift) QFCs have been demonstrated in SiN_x micro-rings at the single-photon level¹¹⁸. Such a scheme has been successfully applied to the Fock-states of single photons emitted by the micropillar QD devices for intra-band QFC¹²², as shown in Fig. 5d. While in these works the QFC chip and QD chip were separate elements, significant advances in hybrid and heterogeneous integration of QDs (to be discussed in the next section), including with SiN_x photonics, points to the potential for realizing QD single photon generation and QFC on a single chip in the future. Such integration could significantly improve output photon flux, by removing intermediate chip-to-fiber and fiber-to-chip coupling steps.

The recent technological breakthroughs in integrated photonics could further improve the performances of on-chip QFC devices. For example, the fully-optimized PPLN micro-ring could be used as an ultra-efficient on-chip frequency converter for single photons¹²³ (Fig. 5e). Another emerging opportunity is the recently-developed AlGaAs on insulator platform. The combinations of large $\chi^{(3)}$ nonlinearity¹²⁴, low propagation loss and the avoidance of two-photon absorptions at C-band wavelengths make it extremely promising for high-performance QFC on-chip. In addition, the material compatibility of AlGaAs with GaAs/AlGaAs droplet-etched QDs⁶⁴ could enable efficient single-photon generations and QFC on the same chip, as illustrated in Fig. 5f. Such a device could avoid the coupling of single photons from sources on one chip to frequency converter on another chip, dramatically improving the overall efficiency of the QFC quantum light sources. To maintain high-conversion efficiencies on-chip, photonic engineering is required to maximize the nonlinearly interacting optical modes at different wavelengths. For the $\chi^{(2)}$ process, e.g., Fig. 5e, periodic poling of the sub- μm domain has recently been demonstrated in TFLN nanophotonic devices¹²³, dramatically improving the three-wave mixing process for the QFC. In a QFC process based on $\chi^{(3)}$,

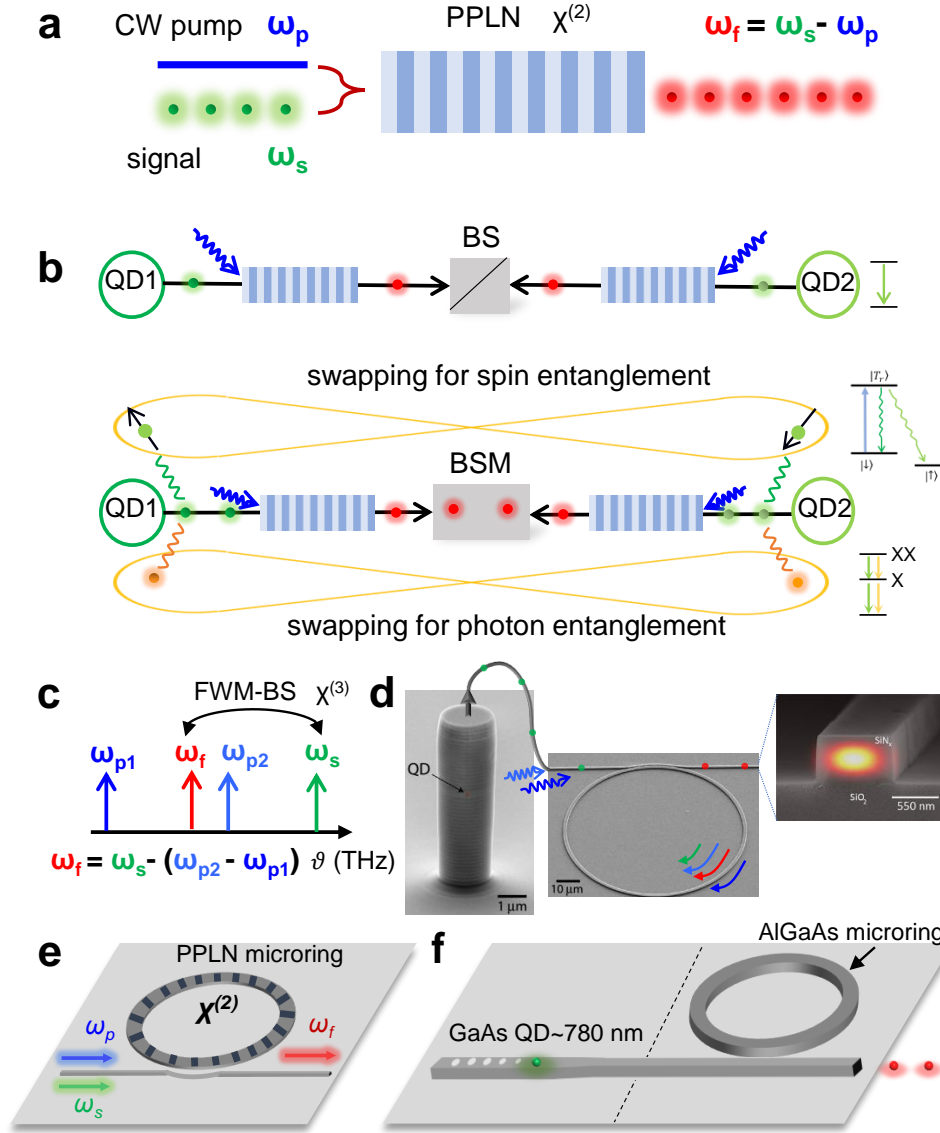


FIG. 5: **Generating telecom band single photons via quantum frequency conversion (QFC).** (a) QFC in periodically poled lithium niobate (PPLN) waveguide through the second-order nonlinear process; (b) The scheme of two-photon interference using QFC telecom single photon (top), as well as the entanglement swapping between the two entangled photon pairs (bottom). (c) Four-wave mixing Bragg scattering (FWM-BS) for visible-telecom QFC; (d) Quantum frequency conversion using the FWM-BS in a hybrid system interfacing III-V quantum emitters and nonlinear silicon nitride resonators¹²², together with the SEM image from fabricated SiN_x waveguide with superimposed fundamental TE mode profile at 1550 nm¹¹⁸; (e) Integrated thin film PPLN circuits for highly-efficient on-chip QFC¹²³; (f) Integrated GaAs QD based quantum light sources with an AlGaAs microring frequency convertor. Reprinted with permission from Refs. [118,122,123].

for instance FWM-BS shown in Fig. 5f, the geometry of the waveguide and cladding material can be carefully engineered so that the pumping lasers, signal and idler are simultaneously resonant with different cavity modes associated to the microring resonator, as successfully demonstrated for both short range (a few nm in 980 nm band) and long-range (980 nm to 1550 nm) QFC processes in SiN_x integrated converters¹¹⁸.

VI. HYBRID INTEGRATED QUANTUM LIGHT SOURCES AT TELECOM WAVELENGTHS

Currently, hybrid integrated quantum photonic circuits are an emerging research frontier, offering opportunities of bringing together quantum emitters, quantum memories, coherent linear and nonlinear operations, and single photon detectors on the same chip. The NIR quantum light sources have been benefited from the hybrid integration via pick-and-place tech-

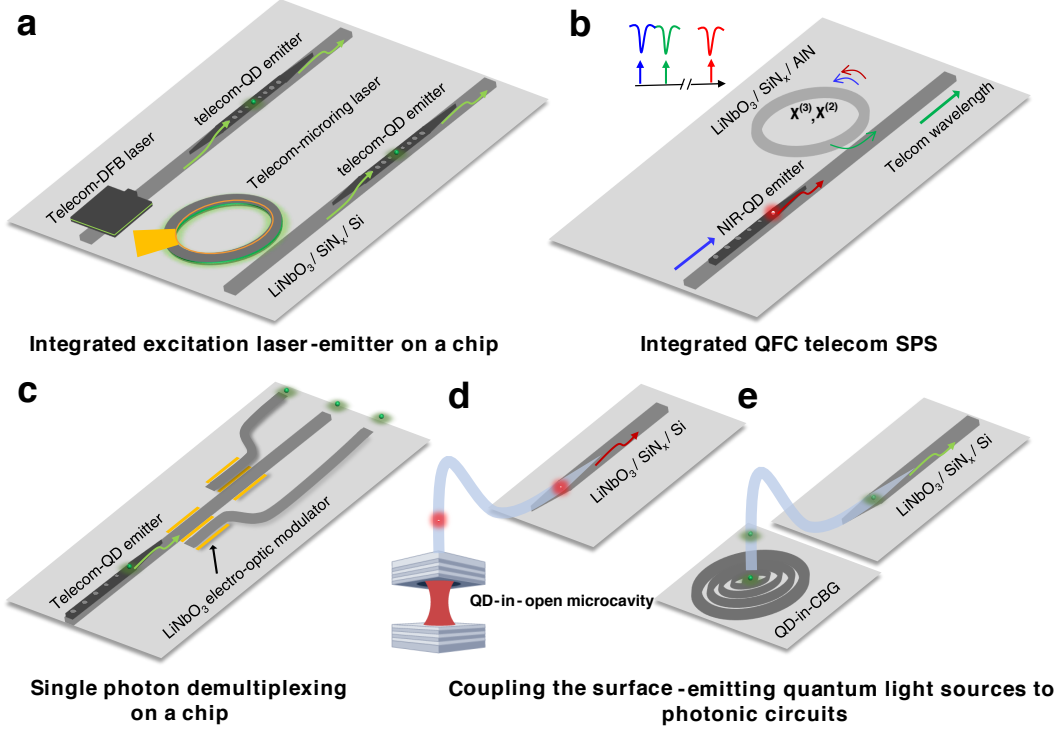


FIG. 6: **Advanced telecom band quantum photonic devices based on hybrid integrations.** (a-c) The sketches of hybrid waveguide-type quantum light sources: telecom band quantum light source with on-chip resonant excitation lasers (a), integrated telecom single photon or entangled photon emitters using on-chip QFC (b), and single photon multiplexing using high performance LiNbO₃ electro-optic modulator (c); (d-e) The sketches of hybrid surface emitting quantum light sources via photonic wire bonding technique: integrating with QD in an open-microcavity (d) or a CBG (e).

nique and wafer-bonding method, as extensively discussed in recent reviews^{125,126}. At telecom bands, pre-characterized single InAs/InP QD SPS have been selectively transferred either on a silicon^{120,127,128} or a LiNbO₃¹²⁹ photonic chips by using a micrometer or submicrometer-sized probe tip¹²⁷ or an adhesive and transparent rubber stamp¹²⁸. However, the hybrid architecture using wafer bonding¹³⁰ has not yet been reported for quantum light source at telecom wavelengths. One remaining problem for this technique is the random position of the emitters and therefore the actual coupling efficiency and yield remain low. Site-controlled emitters mentioned above and the positioning techniques adapted to telecom bands⁷⁹ should be able to resolve these issues in the near future.

Proceeding along this path, hybrid integration may bring a new possibility of realizing functional devices involving different wavelengths of QD emitters, full-blown telecom distributed feedback (DFB)/microring laser, a microresonator quantum frequency convertor, and an electro-optic modulator on a chip, as shown in Figs. 6a-c. It will be particularly interesting for telecom band quantum light sources because the system can provide high-quality micro-lasers for resonant excitations on the same chip (Fig. 6a), integrated telecom single photon or entangle photon emitters using on-chip QFC (Fig. 6b), as well as single-photon multiplexing using high performance LiNbO₃ electro-optic modulator (Fig. 6c).

Besides, photonic wire bonding^{131,132} may offer a solu-

tion for efficient coupling from the light sources to photonic circuits. This is achieved by exploiting direct-write two-photon lithography for in situ fabrication of three-dimensional freeform waveguides/couplers between optical chips (Figs. 6d-e). This technique may provide a universal integration platform for hybrid photonic multi-chip assemblies that combine known-good devices of different materials to high-performance hybrid multi-chips.

VII. PERSPECTIVE

Although tremendous progress has been made towards the development of high-performance telecom wavelength QDs for applications in fiber-based QKD networks and quantum repeaters, there are still important milestone experiments to be pursued to fully release the potential of telecom QD sources. The near-term goal is the experimental demonstration of beating decoy state protocol by using telecom QD sources in a QKD-based quantum communication process. By developing telecom band spin-photon interface with high photon extraction efficiency, spin-spin entanglement over 100 kilometers could be envisioned via entanglement swapping. In the long run, deterministic sources of cluster states with entanglement length up to 50-photons and a generation rate of 2 GHz could enable the realization of high-dimensional cluster states

via cluster fusion, which provides the platform for proof-of-principle experiments for high-rate distribution of entanglements between remote nodes.

The realization of these goals will require both the optimization of existing concepts and the development of new techniques beyond those currently available. For epitaxially grown QDs acting as quantum light sources and spin-photon multi-entanglement cluster states, it is important to improve the single-emitter properties, especially in terms of emission linewidth and photon indistinguishability. The latter is still limited to 40-60% because of enhanced spectral diffusion in O- and C-band QDs due to the detrimental influence of charged defect states in the vicinity of the QDs. Further improvements of the epitaxial layer design and the growth parameter, or even new disruptive growth concepts, are required to overcome these issues and to realize high-performance QDs with Fourier-limited emission linewidths and optimum quantum properties.

Moreover, funneling emission into selected, desirable spatial modes of quantum photonic structures is crucial to maximizing the photon extraction efficiency. For this purpose, deterministic device fabrication technologies for single QD devices, such as various QD positioning and in situ lithography techniques⁶⁷ used mainly for quantum light sources emitting at $\lambda < 1000$ nm, must be extended to process quantum devices emitting at telecom wavelengths. Careful consideration must be paid to the design and fabrication of the photonic structures so that the geometry and the necessary fabrication process minimally affects the as-grown QD optical properties, such as fabrication induced spectral diffusion which limits the photon indistinguishability¹³³.

For QFC quantum light sources, the development of nonlinear candidates capable of high-quality frequency conversion to telecom wavelengths and their integrations with the existing high-performance quantum light sources can be envisaged. The exceptional nonlinear properties of AlGaAs as well as the attractive bright GaAs/AlGaAs QDs at 780 nm have allowed progress with all of these key components and may offer exciting prospects for high performance QFC quantum light sources at telecom wavelengths on a chip. Low-loss thin film LiNbO₃ and SiN_x have also allowed optical nonlinearities at the single photon level, and offered clear advantages with respect to the scalability of the underlying manufacturing processes via the integration with pump lasers and other photonic components. With further technological developments in material growth, photonic design, and integration method, the performances of the telecom band QD devices are steadily im-

proved as quantum light sources and spin-photon interfaces, which plays an increasingly important role in building future solid-state quantum network based on fiber networks.

The cryogenic working temperature ensures the coherent properties of quantum state of the light emitted by QDs. However, for certain applications, e.g., BB84 QKD, room temperature operation is highly preferred for practical reasons while there is no request for the photon coherence and photon indistinguishability. Harnessing exciton localization at defect sites in wide-bandgap semiconductor materials, such as silicon carbide (SiC)¹³⁴ and gallium nitride (GaN)¹³⁵, is rapidly emerging as an alternative means to generate single photons at room temperature. Toward a quantum memory, Er³⁺ ions, which shows both long spin and indistinguishable single photon emission¹³⁶, represent a promising resource for telecom quantum repeater.

Acknowledgements We thank the early contributions to this work from Shiwen Xu and Xiaoying Huang. Y. Y. and J. L. acknowledges the National Key R&D Program of China (2018YFA0306100), the Science and Technology Program of Guangzhou (202103030001), and the National Natural Science Foundation of China (12074442). K. S. acknowledges partial funding support from the NIST-on-a-chip program. S. R. acknowledges financial support from the Federal Ministry of Education and Research (BMBF) via project QR.X (16KISQ014), the German Research Foundation (DFG) via project Re2974-25/1, and the European Union via project SEQUME (20FUN05) that has received funding from the EMPIR programme co-financed by the Participating States and from the European Union's Horizon 2020 research and innovation programme. P. M. gratefully acknowledges the funding by the German Federal Ministry of Education and Research (BMBF) via the project QR.X (No.16KISQ013) and the European Union's Horizon 2020 research and innovation program under Grant Agreement No. 899814 (Europe). Furthermore, we acknowledge financial support by the EMPIR programme (20FUN05 SEQUME), co-financed by the Participating States and from the European Union's Horizon 2020 research and innovation programme. C. M. L. and E. W. acknowledge funding support from the National Science Foundation (grant numbers OMA1936314, PHY1915375, ECCS1933546), the Office of Naval Research (ONR) (grant number N000142012551), the Air Force Office of Scientific Research (AFOSR) (grant number 1021098624), the Maryland ARL quantum partnership (MAQP), and the Quantum Leap Challenge Institute for Robust Quantum Simulation.

* liujin23@mail.sysu.edu.cn

¹ Kimble, H. J. The quantum internet. *Nature* **453**, 1023–1030 (2008).

² Simon, C. Towards a global quantum network. *Nature Photonics* **11**, 678–680 (2017).

³ Fröhlich, B. *et al.* A quantum access network. *Nature* **501**, 69–72 (2013).

⁴ Riedmatten, H. de, *et al.* Long distance quantum teleportation

in a quantum relay configuration. *Physical Review Letters* **92**, 047904 (2004).

⁵ Briegel, H.-J., Dür, W., Cirac, J. I. & Zoller, P. Quantum repeaters: the role of imperfect local operations in quantum communication. *Physical Review Letters* **81**, 5932 (1998).

⁶ Azuma, K., *et al.* Quantum repeaters: From quantum networks to the quantum internet. *arXiv:2212.10820* (2022).

⁷ Żukowski, M., Zeilinger, A., Horne, M. A. & Ekert, A. K.

- "event-ready-detectors" Bell experiment via entanglement swapping. *Physical Review Letters* **71**, 4287–4290 (1993).
- ⁸ Chen, Y.-A. *et al.* Memory-built-in quantum teleportation with photonic and atomic qubits. *Nature Physics* **4**, 103–107 (2008).
 - ⁹ Lvovsky, A. I., Sanders, B. C. & Tittel, W. Optical quantum memory. *Nature photonics* **3**, 706–714 (2009).
 - ¹⁰ Wei, S.-H., *et al.* Towards real-world quantum networks: a review. *Laser & Photonics Reviews* **16**, 2100219 (2022).
 - ¹¹ Hammerer, K., Sørensen, A. S. & Polzik, E. S. Quantum interface between light and atomic ensembles. *Reviews of Modern Physics* **82**, 1041 (2010).
 - ¹² Dutt, M. G. *et al.* Quantum register based on individual electronic and nuclear spin qubits in diamond. *Science* **316**, 1312–1316 (2007).
 - ¹³ Yang, T.-S. *et al.* Multiplexed storage and real-time manipulation based on a multiple degree-of-freedom quantum memory. *Nature Communications* **9**, 1–8 (2018).
 - ¹⁴ Davidson, O. *et al.* Fast, noise-free atomic optical memory with 35% end-to-end efficiency. *arXiv:2212.04263* (2022).
 - ¹⁵ van Loock, P. *et al.* Extending quantum links: modules for fiber- and memory-based quantum repeaters. *Advanced Quantum Technologies* **3**, 1900141 (2022).
 - ¹⁶ Azuma, K., Tamaki, K. & Lo, H.-K. All-photonic quantum repeaters. *Nature Communications* **6**, 1–7 (2015).
 - ¹⁷ Michler, P. *Quantum dots for quantum information technologies*, vol. 237 (Springer, 2017).
 - ¹⁸ Liao, S.-K. *et al.* Long-distance free-space quantum key distribution in daylight towards inter-satellite communication. *Nature Photonics* **11**, 509–513 (2017).
 - ¹⁹ Avesani, M. *et al.* Full daylight quantum-key-distribution at 1550 nm enabled by integrated silicon photonics. *npj Quantum Information* **7**, 93 (2021).
 - ²⁰ Matsui, Y. *et al.* Low-chirp isolator-free 65-GHz-bandwidth directly modulated lasers. *Nature Photonics* **15**, 59–63 (2021).
 - ²¹ He, M. *et al.* High-performance hybrid silicon and lithium niobate Mach–Zehnder modulators for 100 Gbit/s^{−1} and beyond. *Nature Photonics* **13**, 359–364 (2019).
 - ²² Zhang, J., Itzler, M. A., Zbinden, H. & Pan, J.-W. Advances in InGaAs/InP single-photon detector systems for quantum communication. *Light: Science & Applications* **4**, e286 (2015).
 - ²³ Marsili, F. *et al.* Detecting single infrared photons with 93% system efficiency. *Nature Photonics* **7**, 210–214 (2013).
 - ²⁴ Tömm, N. *et al.* A bright and fast source of coherent single photons. *Nature Nanotechnology* **16**, 399–403 (2021).
 - ²⁵ Vajner, D. A. *et al.* Quantum communication using semiconductor quantum dots. *Advanced Quantum Technologies* **5**, 2100116 (2022).
 - ²⁶ Bozzio, M. *et al.* Enhancing quantum cryptography with quantum dot single-photon sources. *npj Quantum Information* **8**, 104 (2022).
 - ²⁷ Anderson, M. *et al.* Gigahertz-clocked teleportation of time-bin qubits with a quantum dot in the telecommunication C-band. *Physical Review Applied* **13**, 054052 (2020).
 - ²⁸ Liu, J. *et al.* A solid-state source of strongly entangled photon pairs with high brightness and indistinguishability. *Nature Nanotechnology* **14**, 586–593 (2019).
 - ²⁹ Gao, W., Fallahi, P., Togan, E., Miguel-Sánchez, J. & Imamoglu, A. Observation of entanglement between a quantum dot spin and a single photon. *Nature* **491**, 426–430 (2012).
 - ³⁰ Delteil, A. *et al.* Generation of heralded entanglement between distant hole spins. *Nature Physics* **12**, 218–223 (2016).
 - ³¹ Cogan, D. *et al.* Deterministic generation of indistinguishable photons in a cluster state. *Nature Photonics* **17**, 324–329 (2023).
 - ³² Schwartz, I. *et al.* Deterministic writing and control of the dark exciton spin using single short optical pulses. *Physical Review X* **5**, 011009 (2015).
 - ³³ Gerardot, B. D. *et al.* Optical pumping of a single hole spin in a quantum dot. *Nature* **451**, 441–444 (2008).
 - ³⁴ Berezovsky, J., Mikkelsen, M., Stoltz, N., Coldren, L. & Awschalom, D. Picosecond coherent optical manipulation of a single electron spin in a quantum dot. *Science* **320**, 349–352 (2008).
 - ³⁵ Tiurev, K. *et al.* High-fidelity multiphoton-entangled cluster state with solid-state quantum emitters in photonic nanostructures. *Physical Review A* **105**, L030601 (2022).
 - ³⁶ Schwartz, I. *et al.* Deterministic generation of a cluster state of entangled photons. *Science* **354**, 434–437 (2016).
 - ³⁷ Coste, N. *et al.* High-rate entanglement between a semiconductor spin and indistinguishable photons. *Nature Photonics* (2023).
 - ³⁸ Schall, J. *et al.* Bright electrically controllable quantum-dot-molecule devices fabricated by in situ electron-beam lithography. *Advanced Quantum Technologies* **4**, 2100002 (2021).
 - ³⁹ De La Giroday, A. B. *et al.* Exciton-spin memory with a semiconductor quantum dot molecule. *Physical Review Letters* **106**, 216802 (2011).
 - ⁴⁰ Economou, S. E., Lindner, N. & Rudolph, T. Optically generated 2-dimensional photonic cluster state from coupled quantum dots. *Physical Review Letters* **105**, 093601 (2010).
 - ⁴¹ Gangloff, D. *et al.* Quantum interface of an electron and a nuclear ensemble. *Science* **364**, 62–66 (2019).
 - ⁴² Tang, J. S. *et al.* Storage of multiple single-photon pulses emitted from a quantum dot in a solid-state quantum memory. *Nature Communications* **6**, 8652 (2015).
 - ⁴³ Tatebayashi, J., Nishioka, M. & Arakawa, Y. Over 1.5 μm light emission from InAs quantum dots embedded in InGaAs strain-reducing layer grown by metalorganic chemical vapor deposition. *Applied Physics Letters* **78**, 3469–3471 (2001).
 - ⁴⁴ Kettler, J. *et al.* Single-photon and photon pair emission from MOVPE-grown In(Ga)As quantum dots: shifting the emission wavelength from 1.0 to 1.3 μm . *Applied Physics B* **122**, 1–6 (2016).
 - ⁴⁵ Srocka, N. *et al.* Deterministically fabricated quantum dot single-photon source emitting indistinguishable photons in the telecom O-band. *Applied Physics Letters* **116**, 231104 (2020).
 - ⁴⁶ Orchard, J. R. *et al.* Silicon-based single quantum dot emission in the telecoms C-band. *ACS Photonics* **4**, 1740–1746 (2017).
 - ⁴⁷ Portalupi, S. L., Jetter, M. & Michler, P. InAs quantum dots grown on metamorphic buffers as non-classical light sources at telecom C-band: A review. *Semiconductor Science and Technology* **34**, 053001 (2019).
 - ⁴⁸ Paul, M. *et al.* Single-photon emission at 1.55 μm from MOVPE-grown InAs quantum dots on InGaAs/GaAs metamorphic buffers. *Applied Physics Letters* **111**, 033102 (2017).
 - ⁴⁹ Liu, Y. *et al.* Electronic coupling in nanoscale InAs/GaAs quantum dot pairs separated by a thin Ga(Al)As spacer. *Nanoscale Research Letters* **10**, 1–6 (2015).
 - ⁵⁰ Nawrath, C. *et al.* Coherence and indistinguishability of highly pure single photons from non-resonantly and resonantly excited telecom C-band quantum dots. *Applied Physics Letters* **115**, 023103 (2019).
 - ⁵¹ Zeuner, K. D. *et al.* On-demand generation of entangled photon pairs in the telecom C-band with InAs quantum dots. *ACS Photonics* **8**, 2337–2344 (2021).
 - ⁵² Marchand, H. *et al.* Metalorganic vapor phase epitaxy of coherent self-assembled InAs nanometer-sized islands in InP (001). *Applied Physics Letters* **71**, 527–529 (1997).
 - ⁵³ Fafard, S., Wasilewski, Z., McCaffrey, J., Raymond, S. & Charbonneau, S. InAs self-assembled quantum dots on InP by molec-

- ular beam epitaxy. *Applied Physics Letters* **68**, 991–993 (1996).
- 54 Sobiesierski, Z. *et al.* As/P exchange on InP (001) studied by reflectance anisotropy spectroscopy. *Applied Physics Letters* **70**, 1423–1425 (1997).
 - 55 Dupuy, E. *et al.* Low density of self-assembled InAs quantum dots grown by solid-source molecular beam epitaxy on InP (001). *Applied Physics Letters* **89**, 123112 (2006).
 - 56 Anantathanasarn, S., Nötzel, R., Van Veldhoven, P., Eijkemans, T. & Wolter, J. Wavelength-tunable (1.55- μm region) InAs quantum dots in InGaAsP/InP (100) grown by metal-organic vapor-phase epitaxy. *Journal of Applied Physics* **98**, 013503 (2005).
 - 57 Takemoto, K., Sakuma, Y., Hirose, S., Usuki, T. & Yokoyama, N. Observation of exciton transition in 1.3–1.55 μm band from single InAs/InP quantum dots in mesa structure. *Japanese journal of Applied Physics* **43**, L349 (2004).
 - 58 Koguchi, N., Takahashi, S. & Chikyow, T. New MBE growth method for InSb quantum well boxes. *Journal of Crystal Growth* **111**, 688–692 (1991).
 - 59 Machnikowski, P. & Jacak, L. Resonant nature of phonon-induced damping of Rabi oscillations in quantum dots. *Physical Review B* **69**, 193302 (2004).
 - 60 Skiba-Szymanska, J. *et al.* Universal growth scheme for quantum dots with low fine-structure splitting at various emission wavelengths. *Physical Review Applied* **8**, 014013 (2017).
 - 61 Ha, N. *et al.* Single photon emission from droplet epitaxial quantum dots in the standard telecom window around a wavelength of 1.55 μm . *Applied Physics Express* **13**, 025002 (2020).
 - 62 Müller, T. *et al.* A quantum light-emitting diode for the standard telecom window around 1,550 nm. *Nature Communications* **9**, 1–6 (2018).
 - 63 Liu, X. *et al.* Vanishing fine-structure splittings in telecommunication-wavelength quantum dots grown on (111)A surfaces by droplet epitaxy. *Physical Review B* **90**, 081301 (2014).
 - 64 Zhai L. *et al.* Low-noise GaAs quantum dots for quantum photonics. *Nature Communications* **11**, 8 (2020).
 - 65 Chellu A. *et al.* Highly uniform GaSb quantum dots with indirect–direct bandgap crossover at telecom range. *APL Materials* **9**, 051116 (2021).
 - 66 Cao X. *et al.* Local droplet etching on InAlAs/InP surfaces with InAl droplets. *AIP Advances* **12**, 055302 (2022).
 - 67 Liu, S., Srinivasan, K. & Liu, J. Nanoscale positioning approaches for integrating single solid-state quantum emitters with photonic nanostructures. *Laser & Photonics Reviews* **15**, 2100223 (2021).
 - 68 Singh, R. & Bester, G. Nanowire quantum dots as an ideal source of entangled photon pairs. *Physical Review Letters* **103**, 063601 (2009).
 - 69 Haffouz, S. *et al.* Bright single InAsP quantum dots at telecom wavelengths in position-controlled InP nanowires: The role of the photonic waveguide. *Nano letters* **18**, 3047–3052 (2018).
 - 70 Zhang, J. *et al.* Planarized spatially-regular arrays of spectrally uniform single quantum dots as on-chip single photon sources for quantum optical circuits. *APL Photonics* **5**, 116106 (2020).
 - 71 Strittmatter, A. *et al.* Lateral positioning of ingaas quantum dots using a buried stressor. *Applied Physics Letters* **100**, 093111 (2012).
 - 72 Große, J., von Helversen, M., Koulas-Simos, A., Hermann, M. & Reitzenstein, S. Development of site-controlled quantum dot arrays acting as scalable sources of indistinguishable photons. *APL Photonics* **5**, 096107 (2020).
 - 73 Chen, Z.-S. *et al.* Bright single-photon source at 1.3 μm based on inas bilayer quantum dot in micropillar. *Nanoscale Research Letters* **12**, 1–6 (2017).
 - 74 Birowosuto, M. D. *et al.* Fast purcell-enhanced single photon source in 1,550-nm telecom band from a resonant quantum dot-cavity coupling. *Scientific Reports* **2**, 1–5 (2012).
 - 75 Kim, J.-H., Cai, T., Richardson, C. J., Leavitt, R. P. & Waks, E. Two-photon interference from a bright single-photon source at telecom wavelengths. *Optica* **3**, 577–584 (2016).
 - 76 Balet, L. *et al.* Enhanced spontaneous emission rate from single inas quantum dots in a photonic crystal nanocavity at telecom wavelengths. *Applied Physics Letters* **91**, 123115 (2007).
 - 77 Barbiero, A. *et al.* High performance single-photon sources at telecom wavelength based on broadband hybrid circular bragg gratings. *ACS Photonics* **9**, 3060–3066 (2022).
 - 78 Kolatschek, S. *et al.* Bright purcell enhanced single-photon source in the telecom O-band based on a quantum dot in a circular bragg grating. *Nano Letters* **21**, 7740–7745 (2021).
 - 79 Xu, S.-W. *et al.* Bright single-photon sources in the telecom band by deterministically coupling single quantum dots to a hybrid circular bragg resonator. *Photonics Research* **10**, B1–B6 (2022).
 - 80 Nawrath, C. *et al.* High emission rate from a purcell-enhanced, triggered source of pure single photons in the telecom C-band. *arXiv:2207.12898* (2022).
 - 81 Holewa, P. *et al.* Scalable quantum photonic devices emitting indistinguishable photons in the telecom C-band. *arXiv:2304.02515* (2023).
 - 82 Takemoto, K. *et al.* An optical horn structure for single-photon source using quantum dots at telecommunication wavelength. *Journal of Applied Physics* **101**, 081720 (2007).
 - 83 Haffouz, S. *et al.* Single quantum dot-in-a-rod embedded in a photonic nanowire waveguide for telecom band emission. *Applied Physics Letters* **117**, 113102 (2020).
 - 84 Jaffal, A. *et al.* InAs quantum dot in a needlelike tapered InP nanowire: a telecom band single photon source monolithically grown on silicon. *Nanoscale* **11**, 21847–21855 (2019).
 - 85 Takemoto, K. *et al.* Telecom single-photon source with horn structure. *Physica Status Solidi C* **5**, 2699–2703 (2008).
 - 86 Lee, C.-M. *et al.* Bright telecom-wavelength single photons based on a tapered nanobeam. *Nano Letters* **21**, 323–329 (2020).
 - 87 Yang, J. *et al.* Quantum dot-based broadband optical antenna for efficient extraction of single photons in the telecom O-band. *Optics express* **28**, 19457–19468 (2020).
 - 88 Sartison, M. *et al.* Deterministic integration and optical characterization of telecom O-band quantum dots embedded into wet-chemically etched Gaussian-shaped microlenses. *Applied Physics Letters* **113**, 032103 (2018).
 - 89 Musiał, A. *et al.* Inp-based single-photon sources operating at telecom C-band with increased extraction efficiency. *Applied Physics Letters* **118**, 221101 (2021).
 - 90 Bremer, L. *et al.* Numerical optimization of single-mode fiber-coupled single-photon sources based on semiconductor quantum dots. *Optics Express* **30**, 15913–15928 (2022).
 - 91 Schlehahn, A. *et al.* A stand-alone fiber-coupled single-photon source. *Scientific Reports* **8**, 1–7 (2018).
 - 92 Musiał, A. *et al.* Plug&play fiber-coupled 73 kHz single-photon source operating in the telecom O-band. *Advanced Quantum Technologies* **3**, 2000018 (2020).
 - 93 Yariv, A. & Yeh, P. *Photonics: optical electronics in modern communications* (Oxford university press, 2007).
 - 94 Lee, C.-M. *et al.* A fiber-integrated nanobeam single photon source emitting at telecom wavelengths. *Applied Physics Letters* **114**, 171101 (2019).
 - 95 Northeast, D. B. *et al.* Optical fibre-based single photon source using inasp quantum dot nanowires and gradient-index lens collection. *Scientific Reports* **11**, 1–9 (2021).

- ⁹⁶ Ates, S. *et al.* Improving the performance of bright quantum dot single photon sources using temporal filtering via amplitude modulation. *Scientific Reports* **3**, 1–7 (2013).
- ⁹⁷ Gröblacher, S., Hill, J. T., Safavi-Naeini, A. H., Chan, J. & Painter, O. Highly efficient coupling from an optical fiber to a nanoscale silicon optomechanical cavity. *Applied Physics Letters* **103**, 181104 (2013).
- ⁹⁸ Gyger, S. *et al.* Metropolitan single-photon distribution at 1550 nm for random number generation. *Applied Physics Letters* **121**, 194003 (2022).
- ⁹⁹ Xiang, Z. H. *et al.* Long-term transmission of entangled photons from a single quantum dot over deployed fiber. *Scientific Reports* **9**, 4111 (2019).
- ¹⁰⁰ Xiang, Z. H. *et al.* A tunable telecom wavelength entangled light emitting diode deployed in an installed fibre network. *Communications Physics* **3**, 121 (2020).
- ¹⁰¹ Anderson, M. *et al.* Quantum teleportation using highly coherent emission from telecom C-band quantum dots. *npj Quantum Information* **6**, 14 (2020).
- ¹⁰² Takemoto, K. *et al.* Quantum key distribution over 120 km using ultrahigh purity single-photon source and superconducting single-photon detectors. *Scientific Reports* **5**, 14383 (2015).
- ¹⁰³ Rickert, L., Kupko, T., Rodt, S., Reitzenstein, S. & Heindel, T. Optimized designs for telecom-wavelength quantum light sources based on hybrid circular bragg gratings. *Optics Express* **27**, 36824–36837 (2019).
- ¹⁰⁴ Barbiero, A. *et al.* Design study for an efficient semiconductor quantum light source operating in the telecom C-band based on an electrically-driven circular bragg grating. *Optics Express* **30**, 10919–10928 (2022).
- ¹⁰⁵ Wells, L. *et al.* Coherent light scattering from a telecom C-band quantum dot. *arXiv:2205.07997* (2022).
- ¹⁰⁶ Wang, H. *et al.* Near-transform-limited single photons from an efficient solid-state quantum emitter. *Physical Review Letters* **116**, 213601 (2016).
- ¹⁰⁷ Lettner, T. *et al.* Strain controlled quantum dot fine structure for entangled photon generation at 1550 nm. *Nano Letters* **21**, 10501–10506 (2021).
- ¹⁰⁸ Dusanowski, Ł. *et al.* Optical charge injection and coherent control of a quantum-dot spin-qubit emitting at telecom wavelengths. *Nature Communications* **13**, 1–8 (2022).
- ¹⁰⁹ Tchegbotareva A. *et al.* Entanglement between a diamond spin qubit and a photonic time-bin qubit at telecom wavelength. *Physical Review Letters* **123**, 063601 (2019).
- ¹¹⁰ You, X. *et al.* Quantum interference between independent solid-state single-photon sources separated by 300 km fiber. *arXiv:2106.15545* (2021).
- ¹¹¹ Arenskötter E. *et al.* Telecom Quantum Photonic Interface for a $^{40}\text{Ca}^+$ Single-Ion Quantum Memory. *arXiv:2211.08841* (2022).
- ¹¹² Fejer, M. M. Nonlinear optical frequency conversion. *Physics Today* **47**, 25–33 (1994).
- ¹¹³ Da Lio, B. *et al.* A pure and indistinguishable single-photon source at telecommunication wavelength. *Advanced Quantum Technologies* **5**, 2200006 (2022).
- ¹¹⁴ De Greve, K. *et al.* Quantum-dot spin-photon entanglement via frequency downconversion to telecom wavelength. *Nature* **491**, 421–425 (2012).
- ¹¹⁵ Weber, J. H. *et al.* Two-photon interference in the telecom C-band after frequency conversion of photons from remote quantum emitters. *Nature Nanotechnology* **14**, 23–26 (2019).
- ¹¹⁶ Ikuta, R. *et al.* Polarization insensitive frequency conversion for an atom-photon entanglement distribution via a telecom network. *Nature Communications* **9**, 1–8 (2018).
- ¹¹⁷ Liu, J. *et al.* Emerging material platforms for integrated micro-cavity photonics. *Science China Physics, Mechanics & Astronomy* **65**, 1–19 (2022).
- ¹¹⁸ Li, Q., Davanço, M. & Srinivasan, K. Efficient and low-noise single-photon-level frequency conversion interfaces using silicon nanophotonics. *Nature Photonics* **10**, 406–414 (2016).
- ¹¹⁹ Moody, G. *et al.* 2022 roadmap on integrated quantum photonics. *Journal of Physics: Photonics* **4**, 012501 (2022).
- ¹²⁰ Aghaeimebodi, S. *et al.* Silicon photonic add-drop filter for quantum emitters. *Optics Express* **27**, 16882–16889 (2019).
- ¹²¹ McGuinness, H. J., Raymer, M. G., McKinstrie, C. J. & Radic, S. Quantum frequency translation of single-photon states in a photonic crystal fiber. *Physical Review Letters* **105**, 093604 (2010).
- ¹²² Singh, A. *et al.* Quantum frequency conversion of a quantum dot single-photon source on a nanophotonic chip. *Optica* **6**, 563–569 (2019).
- ¹²³ Chen, J.-Y. *et al.* Photon conversion and interaction on chip. *arXiv:2105.00275* (2021).
- ¹²⁴ Ho, S. *et al.* Large nonlinear phase shifts in low-loss $\text{Al}_x\text{Ga}_{1-x}\text{As}$ waveguides near half-gap. *Applied Physics Letters* **59**, 2558–2560 (1991).
- ¹²⁵ Kim, J.-H., Aghaeimebodi, S., Carolan, J., Englund, D. & Waks, E. Hybrid integration methods for on-chip quantum photonics. *Optica* **7**, 291–308 (2020).
- ¹²⁶ Elshaari, A. W., Pernice, W., Srinivasan, K., Benson, O. & Zwiller, V. Hybrid integrated quantum photonic circuits. *Nature Photonics* **14**, 285–298 (2020).
- ¹²⁷ Kim, J.-H. *et al.* Hybrid integration of solid-state quantum emitters on a silicon photonic chip. *Nano Letters* **17**, 7394–7400 (2017).
- ¹²⁸ Ota, Y., Iwamoto, S. & Arakawa, Y. Hybrid integrated light sources on silicon assembled by transfer printing. In *2021 IEEE Photonics Conference (IPC)*, 1–2 (IEEE, 2021).
- ¹²⁹ Aghaeimebodi, S. *et al.* Integration of quantum dots with lithium niobate photonics. *Applied Physics Letters* **113**, 221102 (2018).
- ¹³⁰ Davanco, M. *et al.* Heterogeneous integration for on-chip quantum photonic circuits with single quantum dot devices. *Nature Communications* **8**, 1–12 (2017).
- ¹³¹ Billah, M. R. *et al.* Hybrid integration of silicon photonics circuits and inp lasers by photonic wire bonding. *Optica* **5**, 876–883 (2018).
- ¹³² Gehring, H. *et al.* Low-loss fiber-to-chip couplers with ultrawide optical bandwidth. *APL Photonics* **4**, 010801 (2019).
- ¹³³ Liu, J. *et al.* Single self-assembled InAs/GaAs quantum dots in photonic nanostructures: The role of nanofabrication. *Physical Review Applied* **9**, 064019 (2018).
- ¹³⁴ Wang, J. F. *et al.* Bright room temperature single photon source at telecom range in cubic silicon carbide. *Nature Communications* **9**, 4106 (2018).
- ¹³⁵ Meunier, M. *et al.* Telecom single-photon emitters in GaN operating at room temperature: embedment into bullseye antennas. *Nanophotonics* **12**, 1405–1419 (2023).
- ¹³⁶ Ourari, S. *et al.* Indistinguishable telecom band photons from a single erbium ion in the solid state. *arXiv:2301.03564* (2023).